Kovove Mater. 53 2015 295–304
DOI: 10.4149/km_2015_5_295

Annealing effects in hot-deformed Al-Mn-Sc-Zr alloys

M. Vlach[1]*, I. Stulíková[1], B. Smola[1], T. Kekule[1], H. Kudrnová[1], V. Kodetová[1], V. Očenášek[2], J. Málek[3], V. Neubert[4]

[1] *Charles University in Prague, Faculty of Mathematics and Physics, Ke Karlovu 3, CZ-121 16 Prague, Czech Republic*
[2] *SVÚM a.s., Podnikatelská 565, CZ-190 11 Prague, Czech Republic*
[3] *Czech Technical University in Prague, Faculty of Mechanical Engineering, CZ-120 00 Prague, Czech Republic*
[4] *Institut für Materialprüfung und Werkstofftechnik, Freiberger Strasse 1, D-38678 Clausthal-Zellerfeld, Germany*

Received 17 July 2014, received in revised form 18 December 2014, accepted 18 December 2014

Abstract

Microstructure, thermal, electrical and mechanical properties of the hot-extruded and hot-rolled AlMnScZr alloys were studied. The electrical resistometry and microhardness together with differential scanning calorimetry measurements were compared with microstructure development observed by transmission electron microscopy, X-ray diffraction, and electron backscatter diffraction. Fine subgrain or grain structure developed and fine coherent $Al_3(Sc,Zr)$ particles precipitated during hot deformation and subsequent cooling. The distinct resistivity changes are mainly caused by precipitation of Mn-containing particles. The pronounced two-stage development of the $Al_6(Mn,Fe)$-phase precipitation was observed. Nevertheless, the precipitation has a negligible effect on microhardness. The presence of the Mn-containing particles with a size of $\sim$ 50 nm inside subgrains or grains and $\sim$ 2 μm at subgrain or grain boundaries has a significant antirecrystallization effect. The combination of Mn, Sc and Zr additions to Al suppresses recrystallization during isothermal annealing at 550 °C. Hot deformation has no effect on the apparent activation energy values of the Al_3Sc-phase precipitation (Q = 109 kJ mol^{-1}) and Al_6Mn-phase precipitation (Q = 156 kJ mol^{-1}).

K e y w o r d s: Al_3Sc phase, hot extrusion, hot rolling, activation energy, EBSD, DSC

1. Introduction

A small addition of scandium ($c_{Sc} \sim 0.3$ wt.%) and zirconium ($c_{Zr} \sim 0.2$ wt.%) to Al-based alloys increases their recrystallization temperature markedly; it also has a beneficial effect on weldability and corrosion resistance [1–4]. These promising effects are related to the formation of a dense and homogeneous distribution of the $L1_2$-structured $Al_3(Sc,Zr)$ coherent precipitates [5–11]. The complex nanostructure of the $Al_3(Sc,Zr)$ phase in aluminium has been discussed in several recent articles by studies using conventional and high-resolution transmission electron microscopy or atom-probe tomography [12–15].

Manganese is the most widely used transition metal in commercial aluminium alloys [1]. Thus an effect of Mn-containing particles, which were introduced during heat treatment, on properties of the Al-Mn-based alloys has been studied extensively, e.g. Refs. [16, 17]. Precipitation of these particles in Al influences resistivity behaviour significantly [18, 19], although it has a poor effect on microhardness [1, 5, 18, 19]. It was also observed that the fine-grained structure of Al-based alloys helps to accelerate precipitation of Mn-containing particles [17–20]. Despite some investigations of Al-Mn as well as Al-Sc-Zr-based alloys there are considerably less systematic data about Al-Mn-Sc-Zr-based alloys in the literature. Even much fewer articles dealing with properties of these alloys prepared by hot deformation were published, e.g. Refs. [2, 4, 21–23]. The effect of the Mn-, Sc- and Zr-content on recrystallization in binary aluminium alloys has now been partially documented [7, 17, 24–26]. However, an understanding of the complex interactions between concurrent precipitation and recrystallization requires further investigation [15, 24, 26]. The purpose of Sc and Zr added to the Al-Mn-based alloys may be either to stabilize

*Corresponding author: tel.: +420221911659; fax: +420221911618; e-mail address: martin.vlach@mff.cuni.cz

Table 1. The measured and calculated density of the alloys studied

Notation	HE alloy	HR alloy
Measured density (kg m^{-3})	2710 ± 60	2730 ± 80
Calculated density (kg m^{-3})	2729	2729

the microstructure of wrought semi-products (extrusions, rolled plates, forgings, etc.) or to provide extra strength to the alloy through precipitation hardening [2, 24]. Hot deformation of Mn, Sc and Zr containing Al alloys can add other improvements connected with substantial grain refinement and/or can increase stability to elevated temperatures over long periods of time [27, 28].

The aim of the present work was to study the phase transformations and recrystallization behaviour of the hot-deformed Al-Mn-Sc-Zr alloys during isochronal and isothermal annealing. The results of measurements of electrical resistivity, microhardness, differential scanning calorimetry measurements and microstructure investigation were combined.

2. Experimental procedure

Hot-extruded AlMnScZr (HE) alloy and hot-rolled AlMnScZr (HR) alloy were studied. The hot extrusion of cast alloy was performed at 350 ℃ in one step with a reduction 70 : 18. The hot rolling of cast alloy was performed at 300 ℃ in two steps with a total reduction of 90 %. The chemical composition of the alloy is as follows: Mn – 1.38 wt.%, Sc – 0.26 wt.%, Zr – 0.16 wt.%, Fe – 0.10 wt.%, Si – 0.02 wt.% and Al – bal. The hot deformation ensures the low porosity of alloys that might be introduced during casting – cf. the measured and calculated density in Table 1. The values testify very low porosity.

The electrical resistometry measurements were performed at 78 K in liquid N_2 bath and at room temperature (RT) in ethanol (in selected cases only). The electrical resistance was measured using the dc four-point method with a dummy specimen in series within a relative accuracy of $\sim 10^{-4}$. The effect of a parasitic thermo-electromotive force was suppressed by changing the current polarity. The H-shaped specimens machined to dimensions of $2 \times 10 \times 80$ mm^3 were used for these measurements; the length represents the gauge length. The deformation of the electrical field in the vicinity of contacts was estimated yielding the measured resistance accuracy better than $\sim$ 2 %. The accuracy of specimen dimensions measurement is about 3 % that is also the accuracy of the absolute resistivity values [29]. Samples for resistivity measurements were studied during the isochronal annealing procedure (steps of 30 K/30 min) which was performed exactly in the same way as described in Ref. [28]. The annealing was realized in a stirred silicone oil bath up to 240 ℃ followed by quenching into liquid N_2. At higher temperatures, it was performed in an air furnace (samples were wrapped in steel foil) followed by quenching into the water at RT. The ratio RRR of the electrical resistivity at RT to that at 78 K: $RRR = \rho_{RT}/\rho_{78\ K}$ does not depend on the specimen shape and corresponds to a relative Al-matrix purity. The major contribution to temperature independent resistivity component in the alloys comes from solutes in the matrix. Contributions of dislocations or subgrain and grain boundaries in Al-Mn and Al-Sc-Zr-based alloys are two orders of magnitude lower [6, 30–33]. Therefore, a higher RRR value corresponds mainly to higher purity of the matrix, i.e. to a larger amount of solutes bound in precipitates.

The influence of isochronal annealing (steps of 30 K/30 min) and isothermal annealing (at 400 ℃ and 550 ℃) on mechanical properties was studied using Vickers microhardness measurements at RT.

Differential scanning calorimetry (DSC) was performed at heating rates of 1, 2, 5, 10 and 20 K min^{-1} in a Netzsch DSC 200 F3 apparatus. The specimen of mass between 10–15 mg was placed in Al_2O_3 crucible in a dynamic nitrogen atmosphere (40 ml min^{-1}).

X-Ray diffraction (XRD) was performed in Bragg-Brentano geometry on a Bruker D8 Advance diffractometer equipped with Cu X-ray tube and energy dispersive detector at surfaces of the HR and HE alloys in the as-prepared state and after isochronal annealing up to 480 ℃.

The grain structure development was observed by electron backscatter diffraction (EBSD) using a JEOL JSM 7600F scanning electron microscope at 20 kV equipped with a Nordly EBSD detector. Samples were polished in an "ELYANA 230" electrolytic polisher by using a 5 vol.% $HClO_4$ and 1.5 vol.% HNO_3 solution in C_2H_5OH. The results were processed by HKL Channel 5 software equipment.

The structure of the alloys was also determined by metallographic microscope Jena Metaval 85618 and scanning electron microscope (SEM) MIRA I Schottky FE-SEMH equipped with X-ray BRUKER microanalyser. Specimens were prepared by polishing in "Flick Etch Solution" (1.3 vol.% HCl and 0.87 vol.% HF solution in distilled water).

Transmission electron microscopy (TEM) with energy-dispersive-X ray microanalysis and electron diffraction was carried out after selected treatment conditions in the JEOL JEM 2000FX electron microscope. The analysis of precipitated phases was supported by energy-dispersive spectroscopy performed by X-ray BRUKER microanalyser. The specimens for TEM were prepared by the same annealing procedure as those for the electrical resistivity measurements.

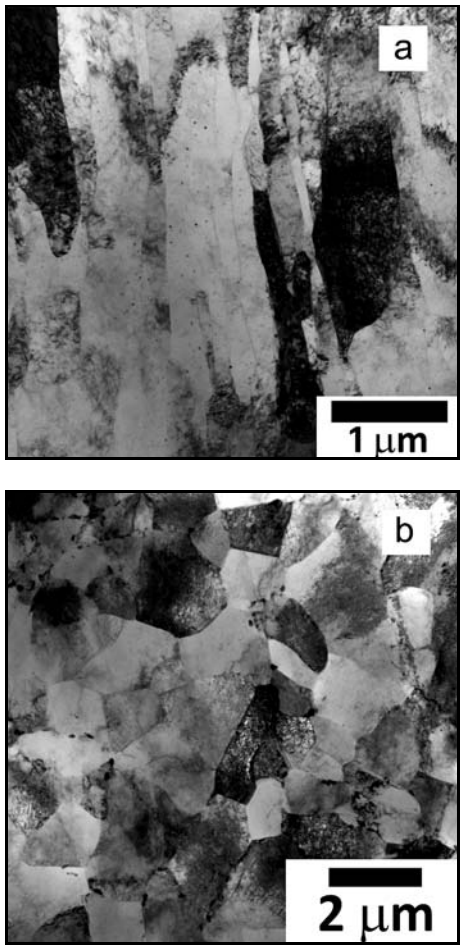

Fig. 1. The as-prepared state of the a) HR alloy and b) HE alloy.

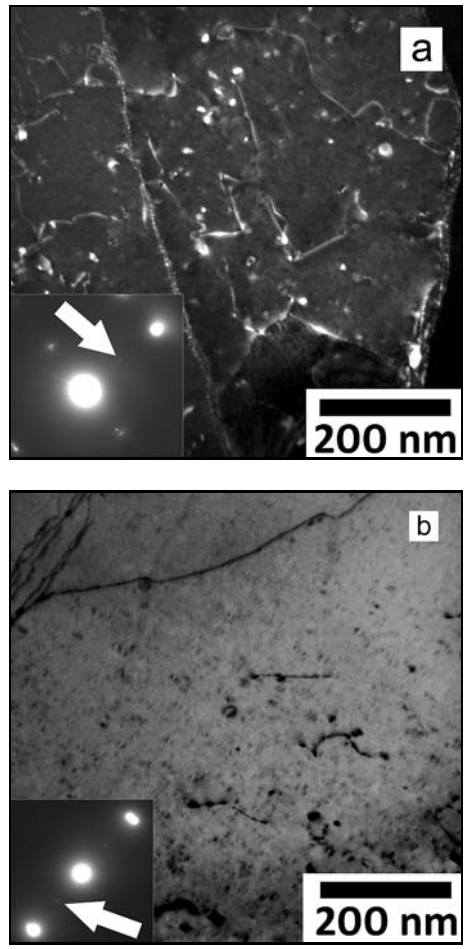

Fig. 2: TEM image and ED pattern (weak spots) of the alloys in the as-prepared state which is characterized by dislocations and coherent $L1_2$-structured particles predominantly situated in (sub)grain interior: a) HR alloy dark field weak beam (DFWB), b) HE alloy bright field (BF).

3. Results and discussion

Fine subgrains or grains ($\sim$ 0.3 μm in width) were observed in the HR alloy (Fig. 1a) elongated in the direction parallel to the hot rolling. A subgrain or grain structure in the range 0.7–2.0 μm was observed in the HE alloy in the cross section of the extrusion direction (see Fig. 1b). Although the contrast of grain or subgrain features (e.g. in Fig. 1) and local changes in their orientation observed by electron diffraction rather suggest their interpretation as subgrains no absolute conclusion could be drawn. Also, EBSD did not provide a decisive information as it was performed at low resolution only due to the short time available for the measurement. Therefore, the subgrain or grain features are termed as (sub)grains throughout the article.

Microstructure observation by TEM revealed a precipitation of the fine coherent Al_3Sc and/or $Al_3(Sc, Zr)$ particles ($L1_2$, cP4 structure) in (sub)grain interiors of both alloys in the as-prepared state. Fig. 2 shows these $L1_2$-structured particles (in typical coffee--bean contrast of coherent particles) and relatively high dislocation density in the HR (Fig. 2a) and HE (Fig. 2b) alloys. The ED patterns of the $L1_2$--structured particles in the alloys are shown in Fig. 2 (see inset).

The dislocation density in the HR alloy seems to be higher than in the HE alloy; the opposite is true for the number density of $L1_2$-structured particles which is noticeably lower in the HR alloy (cf. Figs. 2a and 2b). The particle size estimated from TEM images was (6 $\pm$ 2) nm and (4 $\pm$ 2) nm for the HR and HE alloys, respectively. Taking into account the temperatures and reductions during the hot mechanical treatments it is possible to expect approximately the same volume fraction of $L1_2$-structured particles in both as-prepared alloys. Due to very low particle size the energy dispersive analysis detected only slightly increased content of Sc and Zr in the particle positions. No other type of precipitates was observed by TEM,

Table 2. As-prepared state of the alloys. HV1 values, initial electrical resistivity ρ_0 and parameter RRR

Notation	HV1 (deformation direction)	HV1 (transversal direction)	ρ_0 (nΩ m)	RRR
HR alloy	73.7 ± 0.7	72.8 ± 1.0	48.4 ± 1.0	1.353
HE alloy	75.5 ± 1.9	76.4 ± 0.9	46.7 ± 0.9	1.425

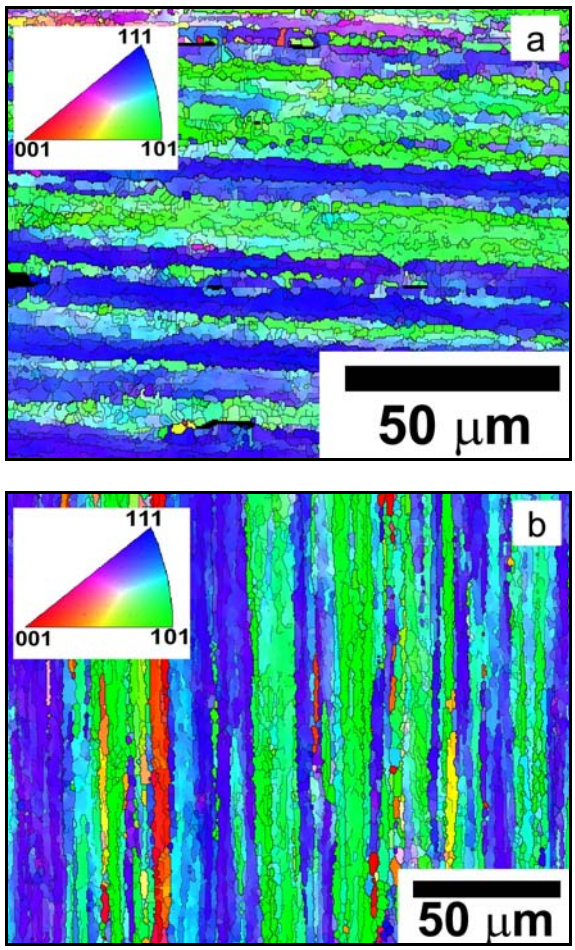

Fig. 3. EBSD picture of the as-prepared state of the alloy: a) HR alloy – plane perpendicular to the rolling direction and b) HE alloy – plane parallel to the extrusion direction.

which means that eventual Mn-containing phase has a very low volume fraction.

A fibrous structure in the transversal direction (TD) was observed in HR alloy and in extrusion direction in HE alloy (representative EBSD maps for the HR alloy – plane perpendicular to the rolling direction and HE alloy – plane parallel to extrusion direction in Figs. 3a and 3b, respectively).

Fibres with final cold rolling texture {112} <111> of Al (blue colour) are present in HR alloy (see Ref. [34]). Almost all other fibres (green colour) have <101> parallel to rolling direction. Only a few fibres exhibit another orientation. About half of fibres (green

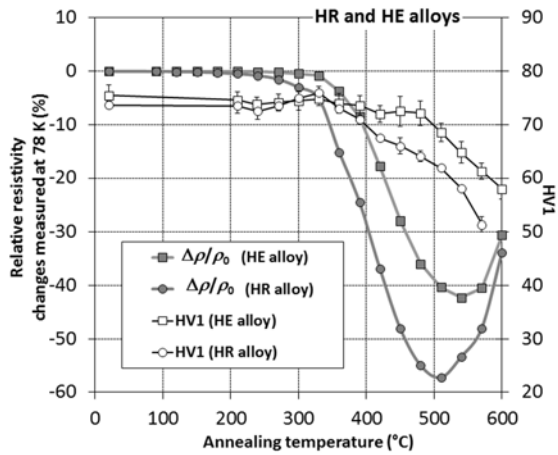

Fig. 4. Isochronal electrical resistivity and microhardness annealing curves of the HR and HE alloy.

colour) may have one of possible draw fibre texture of fcc metals, namely <111> or <001> direction parallel to the extrusion direction. Most of other fibres (blue colour) have orientation near the <111> draw texture.

The initial microhardness HV1, electrical resistivity ρ_0 and RRR values of as-prepared alloys are given in Table 2. The microhardness values of both alloys in the deformation direction and in the transversal direction are the same within experimental error. It indicates the indistinctive influence of the deformation directionality. The lower resistivity value of the HE alloy compared to the HR alloy indicates its higher purity of the Al-matrix. These results are consistent with the denser dispersion of Sc,Zr-containing precipitates in the as-prepared state of the HE alloy. The higher microhardness HV1 values as well as higher RRR values of the HE alloy testify these conclusions.

3.1 Response of the alloys to isochronal annealing

Figure 4 shows isochronal annealing curves of the relative electrical resistivity $\Delta\rho/\rho_0$ changes and microhardness HV1 for the alloys studied. The electrical resistivity decreases from about 210 °C to a minimum at 510 °C for the HR alloy and a minimum at 540 °C for the HE alloy. The HV1 of the HE alloy remains nearly constant up to ∼ 480 °C whereas that of the HR alloy shows a tendency of the slight increase up to ∼ 330 °C. Then microhardness HV1 of the alloys decreases.

Temperature ranges of the largest resistivity chan-

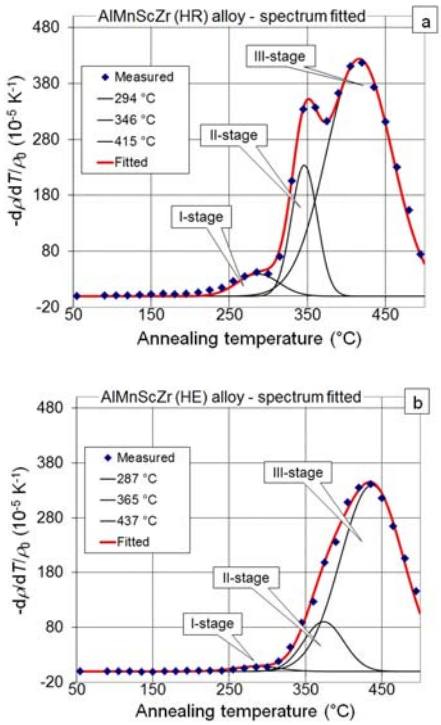

Fig. 5. Spectrum derived as the negative derivative of the isochronal resistivity-annealing curve of the a) HR alloy and b) HE alloy fitted by Gaussian curves of single annealing stages. ρ_0 is the initial value of electrical resistivity.

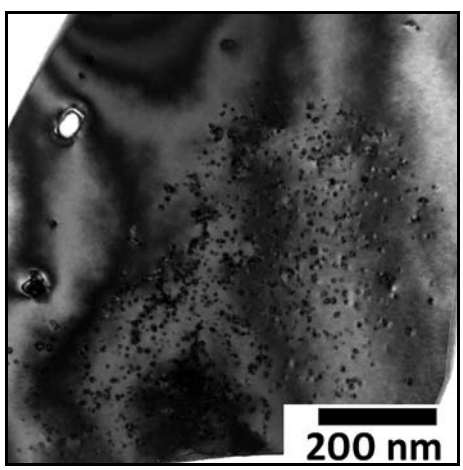

Fig. 6. TEM picture, bright field, [0 0 1] pole of the Al matrix. Notice dense coarsened $Al_3(Sc,Zr)$ particles in (sub)grain interior and few coarse ones in denuded zones developed along (sub)grain boundaries in the HE alloy after annealing up to 540 °C.

ges are better recognized in Fig. 5, where the negative numerical derivatives (spectrum curves) of the annealing curves from Fig. 4 are shown. The obtained spectra can be fitted by Gaussian curves using the method of the least squares, spectrum curve can be then described as a superposition of Gaussian peaks each representing a stage corresponding to precipitation of a certain phase [6, 30, 35]. The area of a Gaussian peak reflects the volume fraction development of the individual phases precipitating. One can see a low temperature stage with a maximum at ∼ 290 °C (I-stage) followed by one stage at ∼ 355 °C (II-stage) and the more pronounced positive stage at ∼ 425 °C (III-stage). The exact temperatures are in the figure insets.

Temperature position of the I-stage does not differ from that observed in the AlMnScZr alloys prepared by different procedures [6, 27, 30]. The I-stage was found there to be caused by the additional precipitation of the $L1_2$-structured Sc,Zr-containing particles. The slight resistivity decrease corresponding to the I-stage in the annealing spectrum of the alloys can be, most probably, ascribed to this process, too. The decrease of electrical resistivity and the distinctness of this stage are more pronounced in the HR alloy, which corresponds to the observed tendency of HV1 value increase up to ∼ 330 °C in the HR alloy. Lower number density of $L1_2$-structured particles observed in as-prepared HR alloy indicates a higher Sc and Zr supersaturation in the solid solution that can lead to the more pronounced additional precipitation of the Al_3Sc and/or $Al_3(Sc,Zr)$-phase particles. Also higher dislocation density in (sub)grains of the as-prepared HR alloy than in the HE alloy can enhance the solute diffusion and consequently this additional precipitation process.

Microstructure observation proved a coarsening of the particles with the $L1_2$-structure during subsequent annealing above 330 °C. The $Al_3(Sc,Zr)$ particles coarsened to diameter 8–15 nm in the (sub)grain interior and denuded zones containing few coarse $Al_3(Sc,Zr)$ particles (∼ 30 nm) developed along (sub)grain boundaries (Fig. 6) in the HE alloy. Similar coarsening of the particles was observed in the HR alloy. The coarsening of the $L1_2$-structured Sc,Zr-containing particles and precipitation of the Mn-containing particles in the AlMnScZr alloys during isochronal annealing at temperatures above 300 °C have been recently described in several publications (e.g. in Refs. [6, 27, 30]).

Diffusivity of Mn atoms in Al is relatively low at temperatures below ∼ 350 °C [36, 37] and Mn atoms can move only on short distances. However, the experiments in the deformed Al-Mn-based alloys show that Mn-containing dispersoids can be formed during isochronal annealing at temperatures starting from ∼ 300 °C [6, 23, 27]. Taking into account the Sc- and Zr-behaviour at comparable temperatures [38, 39] and the known contribution of the unit Mn-, Sc- and Zr-concentration to the resistivity of Al (e.g. [1, 33]) the resistivity development in the alloys at annealing temperatures above ∼ 300 °C must be mainly associated with the change of Mn concentration in the

Al matrix. Least square fitting of the resistivity spectrum above 300 ℃ for both HR and HE alloys by Gaussians revealed summation of two precipitation sub-stages labelled as II- and III-stage (Fig. 5). Linear in-situ annealing in TEM from room temperature done with the same effective rate (1 K min^{-1}) as the isochronal annealing revealed the beginning precipitation of the very small Al_6Mn particles at (sub)grain boundaries starting at ∼ 300 ℃. Small Mn-rich particles in a dense dispersion inside (sub)grains were observed after annealing up to ∼ 340 ℃ whereas the particles at (sub)grain boundaries coarsened considerably (∼ 300 nm). The microstructure of the HR alloy annealed up to 400 ℃ is shown in Fig. 7. Microstructure analysis of the HE alloy also confirms the existence of the Al_6Mn-phase particles with the size of ∼ 30 nm in (sub)grain interiors and hundreds of nanometres at (sub)grain boundaries in the alloy annealed up to 450 ℃. The particles at (sub)grain boundaries coarsen up to size ∼ 2 μm in the HE alloy annealed up to 510 ℃ (Fig. 8) and of size ∼ 3 μm in the HE alloy annealed up to 540 ℃. Lattice parameters of the Al_6Mn and/or $Al_6(Mn,Fe)$ orthorhombic phase in the HE alloy after annealing up to 510 ℃ were determined from ED patterns (inset in Fig. 8) as: a = (0.755 ± 0.006) nm, b = (0.649 ± 0.002) nm, c = (0.887 ± 0.007) nm. XRD analysis (performed earlier in the same alloys similarly treated) also confirms existence of the Al_6Mn and/or $Al_6(Mn,Fe)$ particles in the bulk samples; although peaks were relatively weak due to a small volume fraction, they were clearly indexed on the base of the Al_6Mn and/or $Al_6(Mn,Fe)$ phase [6, 19, 23, 27, 40, 41]. Therefore one can suggest that the II-stage is very probably due to a formation of Mn-containing particles at (sub)grain boundaries and the III-stage is connected with a formation of the Al_6Mn phase in (sub)grain interiors. The similar development of the Mn-containing particles was observed in the previous study of the AlMnScZr alloy prepared by powder metallurgy after extrusion at 350 ℃ (see Ref. [27]). The Mn-containing particles of a size ∼ 50 nm in (sub)grain interiors and hundreds of nanometres at (sub)grain boundaries after the isochronal annealing up to 450 ℃ were observed in that alloy [27]). The two-stage development of the Al_6Mn phase in hot deformed AlMnScZr alloys seems to be generally justified.

Note that precipitation of the Mn-containing particles in the studied alloys has no significant positive effect on hardness (see Fig. 4). The number density of the Al_6Mn particles developed in the HR alloy is probably higher than in the HE one prepared by the same annealing procedure. Microhardness of the HR alloy decreases somewhat faster than that of the HE alloy. This can be explained by a recovery and by a faster coarsening of the Al_3Sc and/or $Al_3(Sc,Zr)$-phase particles due to higher dislocation density and particle size in the as-prepared HR alloy. No recrystallization was observed by EBSD during isochronal annealing up to 570 ℃ either in the HR or in the HE alloy.

Subsequent annealing above 510 ℃ leads to simultaneous coarsening and dissolution of the Al_6Mn particles. The latter increases the concentration of solutes in the Al matrix which leads to the *RRR*

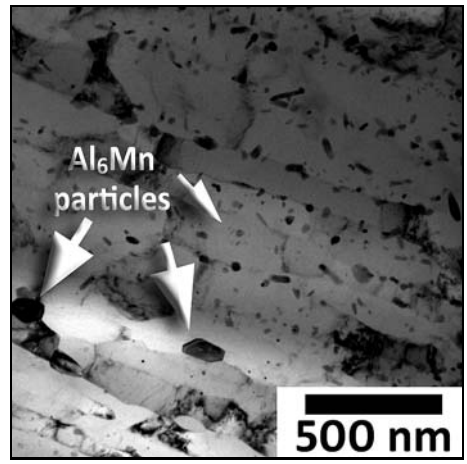

Fig. 7. TEM of the HR alloy annealed up to 400 ℃. Notice Mn-containing particles observed at (sub)grain boundaries and inside (sub)grains.

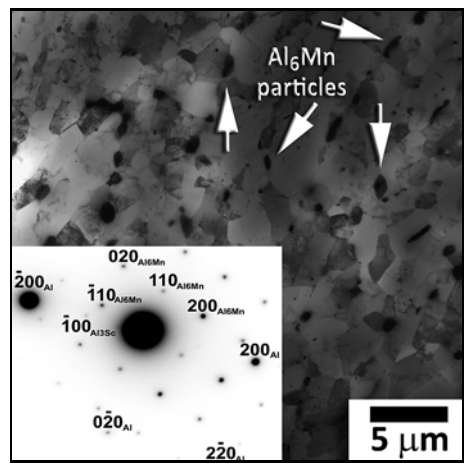

Fig. 8. TEM picture of the HE alloy annealed up to 510 ℃. Notice coarser Mn-containing particles and corresponding reflection of the orthorhombic phase (see inset).

Table 3. *RRR* values after isochronal annealing up to 510 and 570 ℃

Notation	HR alloy	HE alloy
RRR (510 ℃)	2.065	1.861
RRR (570 ℃)	1.826	1.783

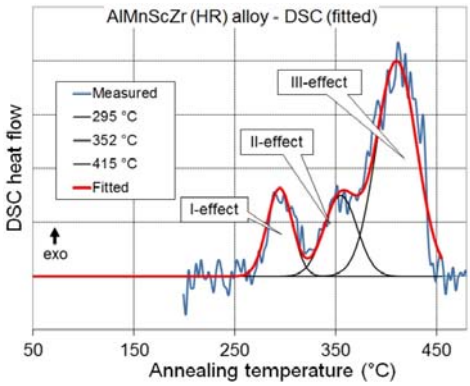

Fig. 9. DSC trace (blue line) in linear heating programme 1 K min^{-1} of the HR alloy fitted up to 450 °C by Gaussian curves (black line) of single exothermal processes.

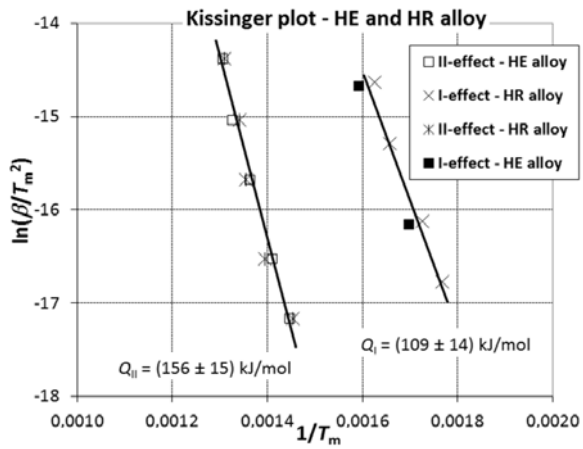

Fig. 10. Kissinger plot of the HR and HE alloy.

value decrease in the alloys isochronally annealed up to 570 °C (see Table 3) compared to the *RRR* value at 510 °C. With respect to the microstructure of the alloys (e.g. Fig. 6) and to the solubility of Sc and Zr in Al at temperatures above 540 °C [1, 2, 36–39], it can be supposed that the dissolution of the $Al_3(Sc,Zr)$ particles can contribute to the resistivity increase and the *RRR* value decrease, too.

3.2 Thermal properties of the hot-deformed alloys during annealing with constant heating rate

DSC measurements were performed in the HR and HE alloys in addition to resistometry and microhardness measurements. Figure 9 shows the DSC curve of the HR alloy at heating rate of 1 K min^{-1} for illustration; that of the HE alloy is similar. Three exothermic effects, marked I–III, can be fitted by Gaussian curves. A weak thermal II-effect was detected only at heating rates of 1 and 5 K min^{-1} in the HR alloy. On the other hand, differential scanning calorimetry revealed only two heat exothermic effects, marked I and III, connected to precipitation processes in the HE alloy. A weak thermal I-effect was detected for heating rates of 2 and 10 K min^{-1} of the HE alloy only. Although some effects were not evaluated due to a small distinctness, it is seen that exothermic effects are connected with negative resistivity changes and with positions of the resistivity spectra stages – compare Figs. 4 and 5 – the maxima of resistivity spectra from Fig. 5 agree well with DSC results from Fig. 9. The observed reactions correspond to precipitation of the Al_3Sc and/or $Al_3(Sc,Zr)$ particles (I-effect), precipitation of the Al_6Mn particles at (sub)grain boundaries (II-effect) and precipitation of the Al_6Mn particles inside (sub)grains (III-effect). The characteristic temperatures T_m of maximum heat flow obtained from DSC measurements of the I- and III-effect are given in Table 4. With increasing heating rate, the temperature T_m shifted to higher temperatures. The markedness of the maximum heat flow in the HR alloy was higher than in the HE alloy as a consequence of the higher supersaturation of Sc atoms and somewhat higher dislocation density in the as-prepared HR alloy.

On the basis of obtained results, the activation energy for individual processes was determined by the Kissinger method [42]. As the value of activation energy determined by this method may differ from the true activation energy of the respective phase formation (the method does not meet all requirements for this, [42]) it is called apparent activation energy in the following text. Figure 10 shows the Kissinger plot in the coordinate system of $[\ln(\beta/T_m^2); 1/T_m]$, where β is the heating rate. From the slope of the plot one obtains the apparent activation energy Q for precipitation of the Al_3Sc and Al_6Mn phases: Q_I = (109 ± 14) kJ mol^{-1} and Q_{II} = (156 ± 15) kJ mol^{-1}, respectively. The calculated apparent activation energy of the Al_3Sc-phase formation is slightly lower than the value for the Al_3Sc phase precipitation determined by Jo and Fujikawa [43] in Al-0.15at.%Sc alloy (Q = 124 kJ mol^{-1}). However, it agrees, within accuracy, with the apparent activation energy Q = (110 ± 11) kJ mol^{-1} in the AlMnScZr alloy prepared by powder metallurgy [23] as well as in the cold-rolled AlMnScZr alloy (Q = (116 ± 9) kJ mol^{-1}) [6]. The apparent activation energy value for Al_6Mn-precipitation corresponds within the obtained accuracy to the value of Q = (152 ± 33) kJ mol^{-1} in the hot-extruded AlMnScZr alloy prepared by powder metallurgy, Q = (162 ± 22) kJ mol^{-1} in the cold-rolled AlMnScZr alloy [6] and Q = 149 kJ mol^{-1} in the AA3000 (AlMnFeSiCu) alloy [44].

Table 4. Characteristic temperatures T_m from DSC measurements

Alloy/process	1 K min^{-1}	2 K min^{-1}	5 K min^{-1}	10 K min^{-1}	20 K min^{-1}
HE alloy/Sc,Zr-containing particles	–	316	–	355	–
HE alloy/Mn-containing particles	422	439	460	480	493
HR alloy/Sc,Zr-containing particles	295	306	330	342	–
HR alloy/Mn-containing particles	415	444	465	473	490

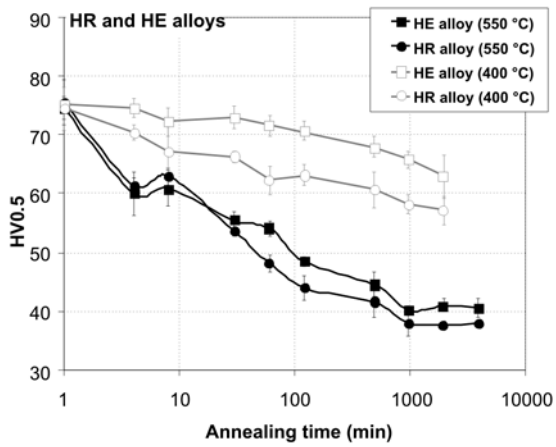

Fig. 11. Microhardness HV0.5 response of the HE and HR alloys to isothermal annealing at 400 °C and 550 °C.

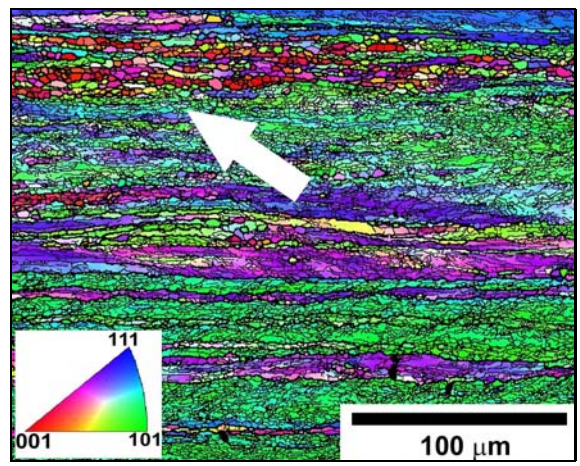

Fig. 12. EBSD map of the HR alloy isothermally annealed at 550 °C/120 min.

3.3 Mechanical properties and microstructure development during isothermal annealing at 400 and 550 °C

The HE and HR alloys were isothermally annealed at 400 °C up to 1 920 min (32 h) and at 550 °C up to 3 840 min (64 h). The results of microhardness HV0.5 measurements are plotted in Fig. 11.

A continuous microhardness decrease was observed in the alloys on isothermal annealing at 400 °C. Microhardness of the HR alloy decreases somewhat faster than that of the HE alloy. This can be explained by a faster recovery and/or by a faster coarsening of the Al_3Sc and/or $Al_3(Sc,Zr)$-phase particles due to the fact that dislocation density in (sub)grains in the as-prepared HR alloy seems to be higher than in the HE alloy. A similar influence of dislocation density was observed in the cold-rolled AlMnScZr alloys prepared by powder metallurgy [27].

No recrystallization at 400 °C was observed in the HR and HE alloys studied here. The EBSD analysis of the alloys after annealing at 400 °C for 1920 min showed a similar (sub)grain structure as in the as-prepared state. The recrystallization in the heavy deformed Al-Mn(-Zr)-based alloys without Sc content was detected during annealing at $\sim$ 400 °C already after 2 h [25, 45]. It indicates that the Al_3Sc- and/or $Al_3(Sc,Zr)$-phase particles have a significant antirecrystallization effect at 400 °C in the studied alloys.

The microhardness annealing curves of the alloys at 550 °C differ from those at 400 °C. Microhardness decreases on annealing at 550 °C somewhat faster than that on annealing at 400 °C and both annealing curves are similar. No changes in grain size and structure were observed in the alloys after annealing 550 °C/30 min. It corresponds to the fact that no recrystallization was proved after isochronal annealing of the alloys up to 570 °C, too. Thus the microhardness HV0.5 decrease after annealing 550 °C/30 min is probably due to recovery effects and a coarsening of the $Al_3(Sc,Zr)$-phase particles in the studied alloys.

Only a partial sporadic recrystallization of the alloys was registered at 550 °C/120 min in the HR alloy (see Fig. 12). Unlike in the HR alloy, no signs of recrystallization were observed in the HE alloy. Explanation of the facts can be connected with the larger (sub)grain size of HE alloy together with higher dislocation density in the as-prepared HR alloy which provides a higher driving force for recrystallization and/or coarsening of the Sc,Zr-containing particles. There is no narrow range of the fast softening in the HR alloy which is typical for recrystallization processes and which was observed, e.g. in the Al-Mn-Zr-based alloys [25, 41, 45].

The fully recrystallized structure of the hot-deformed AlScZr alloy without Mn was clearly ob-

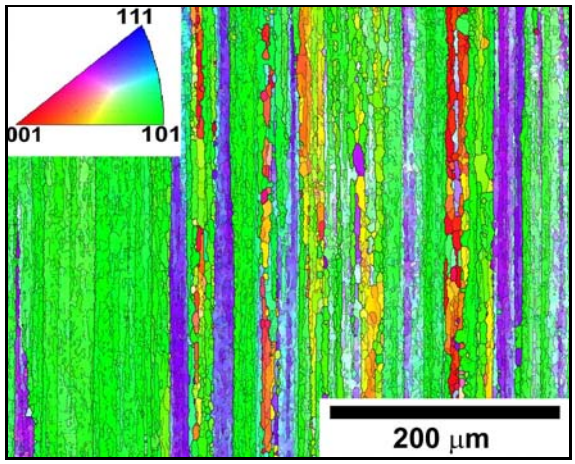

Fig. 13. EBSD map of the HE alloy isothermally annealed at 550 °C/960 min.

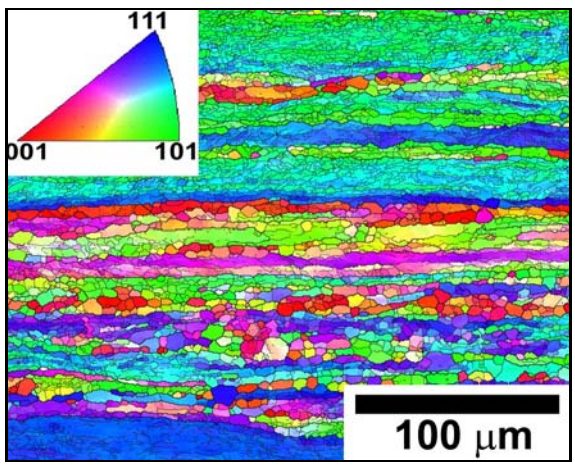

Fig. 14. EBSD map of the HR alloy isothermally annealed at 550 °C/3 840 min.

served after annealing 550 °C/16 h [27]. Contrary to these results only first signs of local recrystallization at 550 °C/960 min were observed in the HE alloy studied here (see Fig. 13). A large improvement of recrystallization resistance due to a combination of Mn, Sc and Zr is evident.

Only a slight coarsening of the recrystallized grains in the HR alloy was observed during annealing at 550 °C for 64 h; the grain structure of the alloy is shown in Fig. 14. On the other hand, microstructure of the HE alloy is more stable until the end of isothermal annealing. No changes in the grain development were observed at 550 °C/3 840 min. It corresponds to constant microhardness values above 16 hours during annealing at 550 °C.

4. Conclusions

From the results of the microstructural observation and mechanical, electrical and thermal properties of the hot-deformed AlMnScZr alloy, it can be concluded:

1) Dense dispersion of very fine coherent spherical particles of the Al_3Sc and/or $Al_3(Sc,Zr)$ phase precipitates in (sub)grain interiors during hot deformation and subsequent cooling.

2) The pronounced two-stage development of the Al_6Mn- and/or $Al_6(Mn,Fe)$-phase precipitation at (sub)grain boundaries and inside (sub)grains was observed. Nevertheless, the precipitation has a negligible effect on hardness. The presence of the Mn-containing particles with the size of $\sim$ 50 nm inside (sub)grains and $\sim$ 2 μm at (sub)grain boundaries has a significant antirecrystallization effect in the alloys studied. The combination of Mn, Sc and Zr additions to Al suppresses recrystallization at 550 °C.

3) Hot deformation has no effect on the apparent activation energy values of the Al_3Sc-phase and Al_6Mn-phase precipitation (inside (sub)grains). The apparent activation energy values of the formation and/or coarsening of the Al_3Sc particles were determined as (109 $\pm$ 14) kJ mol^{-1} for the hot-deformed alloys. The apparent activation energy for the Al_6Mn and/or $Al_6(Mn,Fe)$ phase precipitation was determined as (156 $\pm$ 15) kJ mol^{-1}.

Acknowledgement

The work is a part of activities of the Charles University Research Centre (UNCE) “Physics of Condensed Matter and Functional Materials”.

References

[1] Toropova, L. S., Eskin, D. G., Kharakterova, M. L., Dobatkina, T. V.: Advanced Aluminium Alloys Containing Scandium – Structure and Properties. The Netherlands, Gordon and Breach Science Publisher 1998.

[2] Røyset, J., Ryum, R.: Int. Mater. Rev., *50*, 2005, p. 19. doi:10.1179/174328005X14311

[3] Forbord, B., Hallem, H., Røyset, J., Marthinsen, K.: Mater. Sci. Eng. A, *475*, 2008, p. 241. doi:10.1016/j.msea.2007.04.054

[4] Smola, B., Stulíková, I., Očenášek, V., Pelcová, J., Neubert, V.: Mater. Sci. Eng. A, *462*, 2008, p. 370. doi:10.1016/j.msea.2005.11.075

[5] Vlach, M., Stulíková, I., Smola, B., Žaludová, N.: Mater. Charact., *61*, 2010, p. 1400. doi: 10.1016/j.matchar.2010.10.006

[6] Vlach, M., Stulíková, I., Smola, B. et al.: Mater. Sci. Eng. A, *548*, 2012, p. 27. doi:10.1016/j.msea.2012.03.063

[7] Jia, Z., Røyset, J., Solberg, J. K., Liu, Q.: Trans. Nonferrous Met. Soc. China, *22*, 2012, p. 1866. doi:10.1016/S1003-6326(11)61399-X
[8] Belov, N. A., Alabin, A. N., Eskin, D. G., Istomin-Kastrovskii, V. V.: J. Mater. Sci., *41*, 2006, p. 5890. doi:10.1007/s10853-006-0265-7
[9] Booth-Morrison, C., Dunand, D. C., Seidman, D. N.: Acta Mater., *59*, 2011, p. 7029. doi:10.1016/j.actamat.2011.07.057
[10] Cavaliere, P.: J. Mater. Sci., *41*, 2006, p. 4299. doi: 10.1007/s10853-006-6996-7
[11] Booth-Morrison, C., Seidman, D. N., Dunand, D. C.: Acta Mater., *60*, 2012, p. 3643. doi:10.1016/j.actamat.2012.02.030
[12] Belov, N. A., Alabin, A. N., Matveeva, I. A.: J. Alloys Compd., *583*, 2014, p. 206. doi:10.1016/j.jallcom.2013.08.202
[13] Forbord, B., Lefebvre, W., Danoix, F. et al.: Scripta Mater., *51*, 2004, p. 333. doi:10.1016/j.scriptamat.2004.03.033
[14] Lefebvre, W., Danoix, F., Hallem, H. et al.: J. Alloys Compd., *470*, 2009, p. 107. doi:10.1016/j.jallcom.2008.02.043
[15] Vo, N. Q., Dunand, D. C., Seidman, D. N.: Acta Mater., *63*, 2014, p. 73. doi:10.1016/j.actamat.2013.10.008
[16] Xia, X.: Scripta Metall., *28*, 1993, p. 1213. doi: 10.1016/0956-716X(93)90456-3
[17] Birol, Y.: Scripta Mater., *60*, 2009, p. 5. doi: 10.1016/j.scriptamat.2008.07.047
[18] Cieslar, M., Slámová, M., Uhlíř, J. et al.: Kovove Mater., *45*, 2007, p. 91.
[19] Vlach, M., Smola, B., Stulíková, I., Očenášek, V.: Int. J. Mater. Res., *100*, 2009, p. 420. doi:10.3139/146.110022
[20] Vlach, M., Stulíková, I., Smola, B. et al.: Int. J. Mater. Res., *103*, 2012, p. 814. doi:10.3139/146.110712
[21] Neubert, V., Smola, B., Stulikova, I. et al.: Mater. Sci. Eng. A, *464*, 2007, p. 358. doi:10.1016/j.msea.2007.03.070
[22] Kolář, M., Očenášek, V., Uhlíř, J. et al.: Mater. Sci. Forum, *567–568*, 2008, p. 357. doi: 10.4028/www.scientific.net/MSF.567-568.357
[23] Vlach, M., Stulikova, I., Smola, B. et al.: Acta Phys. Pol. A, *122*, 2012, p. 439.
[24] Jones, M. J., Humphreys, F. J.: Acta Mater., *51*, 2003, p. 2149. doi:10.1016/S1359-6454(03)00002-8
[25] Jia, Z., Hu, G., Forbord, B., Solberg, J. K.: Mater. Sci. Eng. A, *444*, 2007, p. 284. doi:10.1016/j.msea.2006.08.097
[26] Karlík, M., Mánik, T., Slámová, M., Lauschmann, H.: Acta Phys. Pol. A, *122*, 2012, p. 469.
[27] Vlach, M., Stulikova, I., Smola, B. et al.: Mater. Charact., *86*, 2013, p. 59. doi:10.1016/j.matchar.2013.09.010
[28] Vlach, M., Stulikova, I., Smola, B. et al.: Def. Dif. Forum, *334–335*, 2013, p. 161. doi:10.4028/www.scientific.net/DDF.334-335.161
[29] Hájek, M., Veselý, J., Cieslar, M.: Mater. Sci. Eng. A, *462*, 2007, p. 339. doi:10.1016/j.msea.2006.01.175
[30] Vlach, M., Stulíková, I., Smola, B. et al.: J. Alloys Compd., *492*, 2010, p. 143. doi:10.1016/j.jallcom.2009.11.126
[31] Vonbasse, A., Mitchell, E. N.: Phys. Rev., *182*, 1969, p. 712. doi:10.1103/PhysRev.182.712
[32] Ueda, Y., Tamura, H., Hashimoto, E.: J. Phys.-Condens. Matter, *6*, 1994, p. L637. doi:10.1088/0953-8984/6/43/001
[33] Fickett, F. R.: Cryogenics, *11*, 1971, p. 349. doi: 10.1016/0011-2275(71)90036-1
[34] Todayama, A., Inagaki, H.: Mater. Sci. Forum, *495–497*, 2005, p. 603. doi:10.4028/www.scientific.net/MSF.495-497.603
[35] Stulikova, I., Smola, B.: Solid State Phenom., *138*, 2008, p. 57. doi:10.4028/www.scientific.net/SSP.138.57
[36] Knipling, K. E., Dunand, D. C., Seidman, D. N.: Int. J. Mater. Res., *97*, 2006, p. 246. doi:10.3139/146.101249
[37] Forbord, B., Auran, L., Lefebvre, W. et al.: Mater. Sci. Eng. A, *424*, 2006, p. 174. doi:10.1016/j.msea.2006.03.044
[38] Fujikawa, S. I., Sugaya, M., Takei, H., Hirano, K. I.: J. Less-Common Met., *63*, 1979, p. 63. doi:10.1016/0022-5088(79)90211-X
[39] Kang, Y., Pelton, A. D., Chartrand, P., Fuerst, C. D.: Calphad, *32*, 2008, p. 413. doi:10.1016/j.calphad.2008.03.002
[40] Vojtěch, D., Saksl, K., Verner, J., Bártová, B.: Mater. Sci. Eng. A, *428*, 2006, p. 188. doi:10.1016/j.msea.2006.05.017
[41] Birol, Y.: J. Alloys Compd., *471*, 2009, p. 122. doi: 10.1016/j.jallcom.2008.04.005
[42] Starink, M. J.: Thermochim. Acta, *404*, 2003, p. 163. doi: 10.1016/S0040-6031(03)00144-8
[43] Jo, H., Fujikawa, S. I.: Mater. Sci. Eng. A, *171*, 1993, p. 151. doi:10.1016/0921-5093(93)90401-Y
[44] Luiggi, N. J.: Metall. Mater. Trans. B, *28*, 1997; p. 149. doi: 10.1007/s11663-997-0137-9
[45] Liu, W. C., Radhakrishnan, B.: Materials Letters, *64*, 2010, p. 1829. doi:10.1016/j.matlet.2010.05.046